Biosensors and Bioelectronics 126 (2019) 800–805

Contents lists available at ScienceDirect

Biosensors and Bioelectronics

journal homepage: www.elsevier.com/locate/bios

Improved ELISA for tumor marker detection using electro-readout-mode based on label triggered degradation of methylene blue

Dongsheng Zhang, Weixiang Li, Zhanfang Ma*, Hongliang Han*

Department of Chemistry, Capital Normal University, Beijing 100048, China

ARTICLE INFO

Keywords:
ELISA
Degradation
Hemin
Carbohydrate antigen 125
Electro-readout mode

ABSTRACT

Enzyme-linked immunosorbent assay (ELISA), a gold-standard method for protein detection, has been widely utilized in disease diagnosis. Nevertheless, the method is constrained by its dependence on a colorimetric readout that, due to its relatively low sensitivity, prevents its use in tumor marker detection. Here we demonstrate an ELISA that incorporates an electro-readout mode in place of a colorimetric readout to achieve ultrasensitive and convenient tumor marker detection. Briefly, because hemin molecules supported by carbon sphere (CS) can catalyze dye degradation upon H_2O_2 addition, CS incorporating hemin was employed as a label. A hydrogel of sodium alginate-graphene oxide (SA-GO) affixed to an electrode was utilized as a support matrix to immobilize methylene blue (MB) for electrochemical signal generation. Using an ELISA like approach, a solution containing H_2O_2 was added to wells of 96-well plates containing preformed sandwiched immunocomplexes comprised of analyte, capture monoclonal antibody and signal antibody labeled with CS-supported hemin. When the hydrogel-modified electrode was immersed into a well containing a solution containing analyte immunocomplexes, the degradation of MB on the electrode was immediately triggered by label present within the immunocomplexes, resulting in a signal decrease dependent upon analyte concentration. Cancer antigen 125 was used as a model analyte to evaluate the improved ELISA. The calculated limit of detection was 0.048 mU mL^{-1}, which was over six-fold more sensitive than traditional ELISA, indicating that this strategy greatly improves ELISA sensitivity and holds great promise for the quantitative determination of biomarkers for use in clinical diagnosis.

1. Introduction

It is increasingly important to seek facile, affordable, highly sensitive, and portable technologies for the quantitative detection of target proteins in clinical analyses and medical diagnostics. (Bui et al., 2015; Tang and Ma, 2017; Ye et al., 2017; Zhu et al., 2014). As a gold standard of protein detection, enzyme-linked immunosorbent assays (ELISA) have been broadly accepted as a technology for measuring target protein concentrations, owing to the method's sensitivity, high specificity, and wide applicability (Li et al., 2017; Linardy et al., 2016; Yu et al., 2018). Despite its pervasive application, conventional ELISA using protein enzymes as biocatalysts to generate colored readout products has relatively low sensitivity, ranging from μg mL^{-1} to ng mL^{-1}. Thus, conventional ELISA cannot detect proteins at very low concentrations, a strict requirement for early cancer diagnosis. Thus, a new strategy is urgently needed to overcome the limitations of conventional ELISA.

For conventional ELISA, a detectable color signal is generated from biocatalysts (typically, horseradish peroxidase or alkaline phosphatase) which are conjugated to antibodies that specifically bind directly or indirectly to analyte and catalyze the conversion of substrates into colored molecules. Obviously, the performance of enzymes is vital to their detection sensitivity. Therefore, various appropriate strategies for improving the performance were carried out with following two considerations: 1) Increasing the amount or activity of immobilized enzyme to facilitate the color reaction (Chen et al., 2014; Huang et al., 2016; Qu et al., 2014); 2) Employing nanomaterials with much higher catalytic efficiency than obtained using natural enzymes to serve as enzyme mimics to enhance the color signal (Arya and Estrela, 2018; Ye et al., 2017; Zhang et al., 2018a, 2018b). Although these strategies generate suitably high sensitivity for qualitative detection, this colorimetric readout mode still possesses many drawbacks that greatly limit ELISA applications for low-level analyte detection. Specifically, real samples must always be diluted to reduce optical background. However, this will bring some problems. Firstly, sample dilution results in an unsatisfactory analyte detection threshold (by dilution factor) (Vallée-

* Corresponding authors.
E-mail addresses: mazhanfang@cnu.edu.cn (Z. Ma), hanhongliang@cnu.edu.cn (H. Han).

https://doi.org/10.1016/j.bios.2018.11.038
Received 17 August 2018; Received in revised form 24 November 2018; Accepted 26 November 2018
Available online 07 December 2018
0956-5663/

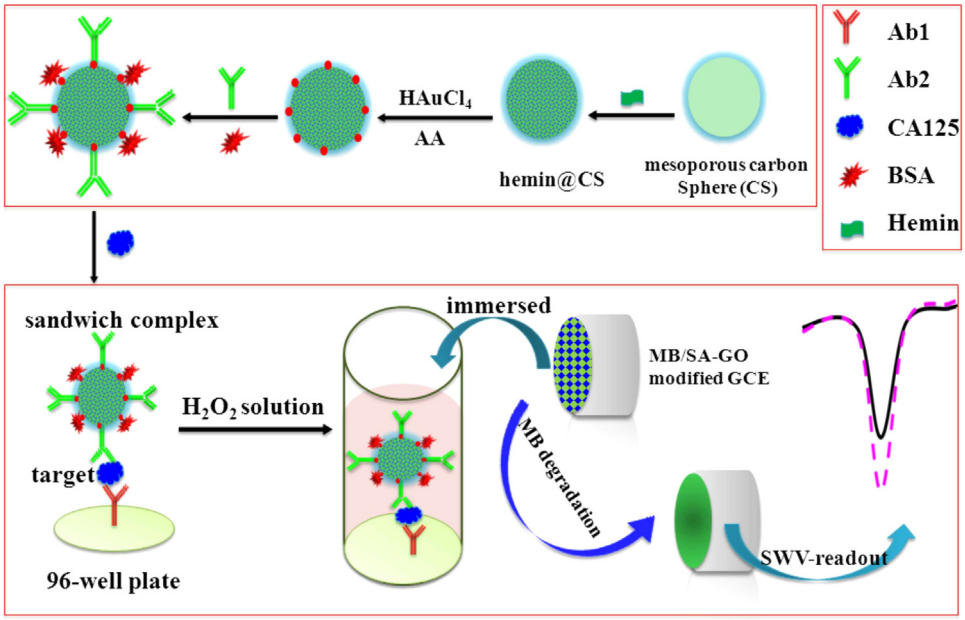

Scheme 1. Schematic representation of the immunosensor for the detection of CA125.

Bélisle et al., 2012). Secondly, in some cases, once samples are diluted, the limit of detection of conventional ELISA cannot meet the requirements of targets detection (Clement et al., 2012; Wang et al., 2016).

Recently, the introduction of novel signal output modes has been an attractive strategy to improve ELISA (Arya and Estrela, 2018; Luo et al., 2018; Shao et al., 2017). To our knowledge, an electro-readout mode possessing advantages of high sensitivity and inherent simplicity would be a promising prospective analytical technique (Arya and Estrela, 2018; Juang et al., 2018; Wang et al., 2018). In this work, we designed an improved ELISA based on the label triggered degradation of methylene blue by replacing the conventional colorimetric readout mode with an electro-readout mode (Scheme 1). In addition, in place of a natural enzyme, a carbon sphere-supported hemin (CS@hemin) possessing the intrinsic peroxidase-like activity was utilized as the label to activate H_2O_2 to generate hydroxyl radicals to effectively catalyze the degradation of methylene blue (MB) (Jiang et al., 2016; Wang et al., 2017; Yao et al., 2015, 2014). Gold nanoparticles (AuNPs) on the surface of CS@hemin were used to immobilize the labeling antibody. Meanwhile, MB was absorbed by a hydrogel of sodium alginate (SA) and graphene oxide (GO) affixed to a glass carbon electrode (GCE), acting as redox species for the electrical signal readout (Li et al., 2013; Thakur et al., 2016; Zhang et al., 2018a, 2018b). Cancer antigen 125 (CA125) was chosen as the model analyte, due to its importance in the detection of ovarian cancer. Obviously, characteristics of two indispensable process steps in this assay synergize to boost sensitivity over that of conventional ELISA: 1) An electrical output signal that possesses inherently higher sensitivity and more rapid development than the enzymatic colorimetric signal readout used in conventional ELISA; 2) The use of CS@hemin, a label possessing superior catalytic efficiency for MB degradation to improve electrochemical signal generation. The calculated limit of detection (LOD) for CA125 was as low as 0.048 mU mL^{-1} (S/N = 3), demonstrating that the modified ELISA was over six orders of magnitude more sensitive than traditional ELISAs (Al-Ogaidi et al., 2013; Hermsen et al., 2007; Sok et al., 2009). Therefore, these results illustrate the great potential of this modified ELISA for facile and sensitive detection of protein targets.

2. Experimental section

2.1. Materials and reagents

Cancer antigen 125 (CA125), CA125 antibody (Ab1, Ab2), Cancer antigen 199 (CA199) and Cancer antigen 242 (CA244) were purchased from Shanghai Linc-Bio Science Co. Human immunoglobulin G (IgG) was obtained from Chengwen Biological Company (Beijing, China). Ascorbic acid (AA), sodium alginate (SA), graphene oxide (GO), bovine serum albumin (BSA) and human serum albumin (HSA) was purchased from Sigma. Human serum samples were obtained from Beijing Genia Biotechnology Company (China). $HAuCl_4{\cdot}XH_2O$ and hemin were purchased from Alfa Aesar. Glucose (Glc) was purchased from Beijing Chemical Reagents Company (China). Methylene blue (MB) was purchased from Acros Organics. Ultrapure water (18.0 MΩ cm) was used throughout the experiments.

2.2. Apparatus

All electrochemical measurements were performed on a three-electrode system (CHI832 electrochemical workstation, Chenhua Instruments Co., Shanghai, China): a glass carbon electrode as working electrode (GCE, 3 mm in diameter), an Ag/AgCl electrode as reference electrode and a platinum wire as counter electrode. X-ray photoelectron spectroscopy (XPS) was obtained on an Escalab 250 × -ray Photoelectron Spectroscope (Thermofisher, American). Scanning electron microscope (SEM) images and energy disperse spectroscopy (EDS) were carried out with a Hitachi SU8010 SEM. The transmission electron microscopy (TEM) images were obtained with a Hitachi (H7650, 80 kV) TEM. UV spectrophotometry was carried out on a UV-2550 UV–vis spectrophotometer (Shimadzu, Japan). The water used was purified through an Olst ultrapure K8 apparatus.

2.3. Synthesis of the label

CS was synthesized by hydrothermal synthetic approach as the previous work (Ceyhan et al., 2015). Briefly, 4 mL glucose (1%) was dissolved in 40 mL water and reacted under hydrothermal conditions at 180 °C for 6 h. The product was purified by washing with water and ethanol alternatively and then collected by centrifugation. The obtained carbon spheres were dried by freeze-dryer for further use.

CS@hemin was prepared by mixing carbon spheres aqueous solution (2 mL, 1 mg mL^{-1}) with an equal volume of hemin methanol solution (2 mL, 1 mg mL^{-1}) under ultrasonication for 30 min. The product was collected by centrifugation after washing with methanol and then dispersed in 2 mL water. $HAuCl_4$ (40 μL, 1 wt%) and ascorbic acid (30 μL, 5 mM) were added into the above solution successively and then stirring for 30 min. After washing with water, the resulting CS@hemin/AuNPs were dispersed in 2 mL PBS (pH = 7.5, 0.1 M). Subsequently, the diluted Ab2 were added into the suspension and stirring carefully for 12 h at 4 °C, then, which were blocked with BSA solution (1 wt%) to prevent the nonspecific adsorption.

2.4. Preparation of the MB/SA&GO hydrogel modified electrode

Firstly, a GCE with a diameter of 3 mm was polished carefully and then washed thoroughly with water and ethanol to create a mirror-like surface. Next, 10 μL of a mixture of SA and GO, prepared by mixing equal volume of GO (1 mg mL^{-1}) and SA (0.2 wt%), was added onto the GCE and followed by drying at 37°C. After that, 80 μL of $CaCl_2$ (20 mM) was added and reacted for 15 min to ensure completion of calcium ion cross-linking of the SA/GO hydrogel. The modified GCE was washed with water for three times and then immersed in methylene blue (MB) solution for saturated absorption. Finally, each MB/SA/GO hydrogel modified electrode was obtained after alternative washing with water, PBS and H_2O_2 solution for several times.

2.5. Detection of CA125

First, anti-CA125 (Ab1) (100 μL per well, 5 μg mL^{-1} in CB buffer pH 9.6) was coated on the 96-well plates at 4 °C overnight. After washing the plates three times with PBST washing buffer (10 mM PBS, pH 7.4, 0.3% (v/v) tween 20), the plates were blocked with 300 μL blocking buffer (3% BSA in PBST) for 2 h in an incubator chamber at 37 °C. Then, the CA125 antigen standards or diluted human plasma sample (1% BSA in PBST, pre-diluted 3 folds) were added and then incubated in an incubator chamber at 37 °C for 1 h. After washed with PBST for three times, 100 μL the obtained immunoprobe solution was added into the plates and incubated at 37 °C for another 1 h. After washed three times, H_2O_2 (100 μL per well, 0.10 M) was added. The modified electrode was immediately immersed into the well and incubated at room temperature for 15 min. Finally, the electrochemistry signal was detected with electrochemical workstation after washed with water. The square wave voltammetry (SWV) measurement from −0.5–0.1 V (vs. Ag/AgCl) was conducted with the obtained electrode in the 0.1 M PBS (pH 7.5).

3. Result and discussion

3.1. Synthesis and characterization

CS with uniform size of 200 nm were prepared from a glucose solution by hydrothermal method as previously reported (Fig. 1A) (Sun and Li, 2004; Xu et al., 2012). FTIR spectrum was applied to identify the CS functional groups (Fig. 1B). Bands at 1710 and 1620 cm^{-1}, due to C=O and C=C vibrations respectively, demonstrated the formation of aromatic rings during hydrothermal treatment (Sakaki et al., 1996; Sun and Li, 2004). Bands in the 3030 cm^{-1} and within the range of 1000–1300 cm^{-1}, demonstrated the formation of hydrogel bonding, C-OH stretching and OH bending vibrations, which improved the hydrophilicity and stability of CS in an aqueous system. Next, CS@hemin was obtained simply by mixing CS with hemin in the methanol under ultra-sonication. This process created hemin-containing CS with the intrinsic peroxidase-like activity of hemin for catalyzing MB dye degradation in the presence of H_2O_2; meanwhile this process maximized homogeneous dispersal of catalytically active hemin within the aqueous solution and minimized the formation of catalytically inactive hemin dimers. (Jiang et al., 2016; Wang et al., 2017; Yao et al., 2015, 2014). To achieve hemin attachment to CS, it is highly likely that hemin molecules were adsorbed onto the surfaces of carbon spheres through π-π stacking interactions involving aromatic groups within hemin molecules. UV–vis absorption spectra of free hemin, the mixture of hemin and CS, and the CS@hemin conjugate showed nearly the same sharp absorption peak at 400 nm (Fig. 1C). The absorption band was in accordance with that of monomeric hemin in methanol, indicating that the adsorbed hemin molecules on carbon spheres were monomeric (Guo et al., 2011; Xue et al., 2012).

The composite of CS@hemin and gold nanoparticles (CS@hemin/AuNPs) was synthesized via the reaction of $HAuCl_4$ with the reducing agent ascorbic acid in aqueous solution at room temperature (Ma et al., 2015). The formation of CS@hemin/AuNPs was confirmed by TEM (Fig. 1D), which indicated that CS particles were covered with a uniform shell of gold nanoparticles for the immobilization of antibodies. Moreover, X-ray photoelectron spectroscopy (XPS) was utilized to further confirm the successful preparation of CS@hemin/AuNPs. As displayed in Fig. 1E, the Au4f, C1s, N1s, O1s and Fef2p3 were observed from the complete spectral survey, confirming the existence of hemin (N1s, Fef2p3) and AuNPs (Au4f). These results suggest that CS@hemin/AuNPs were generated successfully.

GCE were first modified with hydrogel composed of SA and GO (with Ca^{2+} as the crosslinking agent), then MB molecules were absorbed by the hydrogel. Electrode-modification processes that resulted in attachment of hydrogel to electrode were confirmed by SEM. (Fig. S1). The clean GCE modified with the mixture of sodium alginate and graphene oxide was rough (Fig. S1B). After treatment with Ca^{2+}, the surfaces became much rougher and a porous structure was formed (Fig. S1C). Then the obtained electrode was immersed in the aqueous MB solution, a membrane with rill-like folds was formed (Fig. S1D). EDS was next used to further demonstrate the modification processes. Compared with the hydrogel modified electrode without MB (Fig. S2), N and S elements were found on the modified electrode only after the MB adsorption (Fig. S3). Therefore, N and S elements were derived from MB, indicating a successful modification process. In addition, electrochemical impedance spectra (EIS) and cyclic voltammetry measurement (CV) were used to monitor changes in interface properties among the various modification layers (Supplementary material).

3.2. Catalytic performance of CS@hemin

To study the catalytic performance of CS@hemin, 3,3,5,5-tetramethylbenzidine (TMB) was used as a peroxidase substrate (Fig. 2A). In the presence of H_2O_2, CS@hemin nanocomposite reacted with TMB to produce oxidized TMB (blue) with an absorbance maximum at 652 nm (Wei and Wang, 2013; Zhang et al., 2008), demonstrating that CS@hemin can be employed as an effective peroxidase mimic for TMB oxidation. To further demonstrate the peroxidase-like property of CS@hemin, this experiment was repeated utilizing other peroxidase substrates such as diazo-aminobenzene (DAB) and o-phenylenediamine (OPD). We observed that CS@hemin could catalyze the oxidation of DAB and OPD to form products with different colors (Garcia-Viloca et al., 2004; Kim et al., 2010). These results indicate that CS@hemin inhibits peroxidase-like activity towards typical peroxidase substrates.

In order to further investigate the catalytic activity of CS@hemin, MB decomposition experiments (Fig. 2B) were performed that MB alone was barely degraded in the presence of H_2O_2 (curve a). When hemin and H_2O_2 were present, the degree of degradation was little where by only about 6.7% of MB was removed in 60 min (curve b). In the presence of CS@hemin, about 19.8% of MB was absorbed from the aqueous solution (curve c). Remarkably, 55.3% of MB was eliminated in the presence of CS@hemin and H_2O_2 (curve d), the highest level of removal was observed. Taken together, these results demonstrated that the introduction of carbon spheres can substantially improve the catalytic activity of hemin.

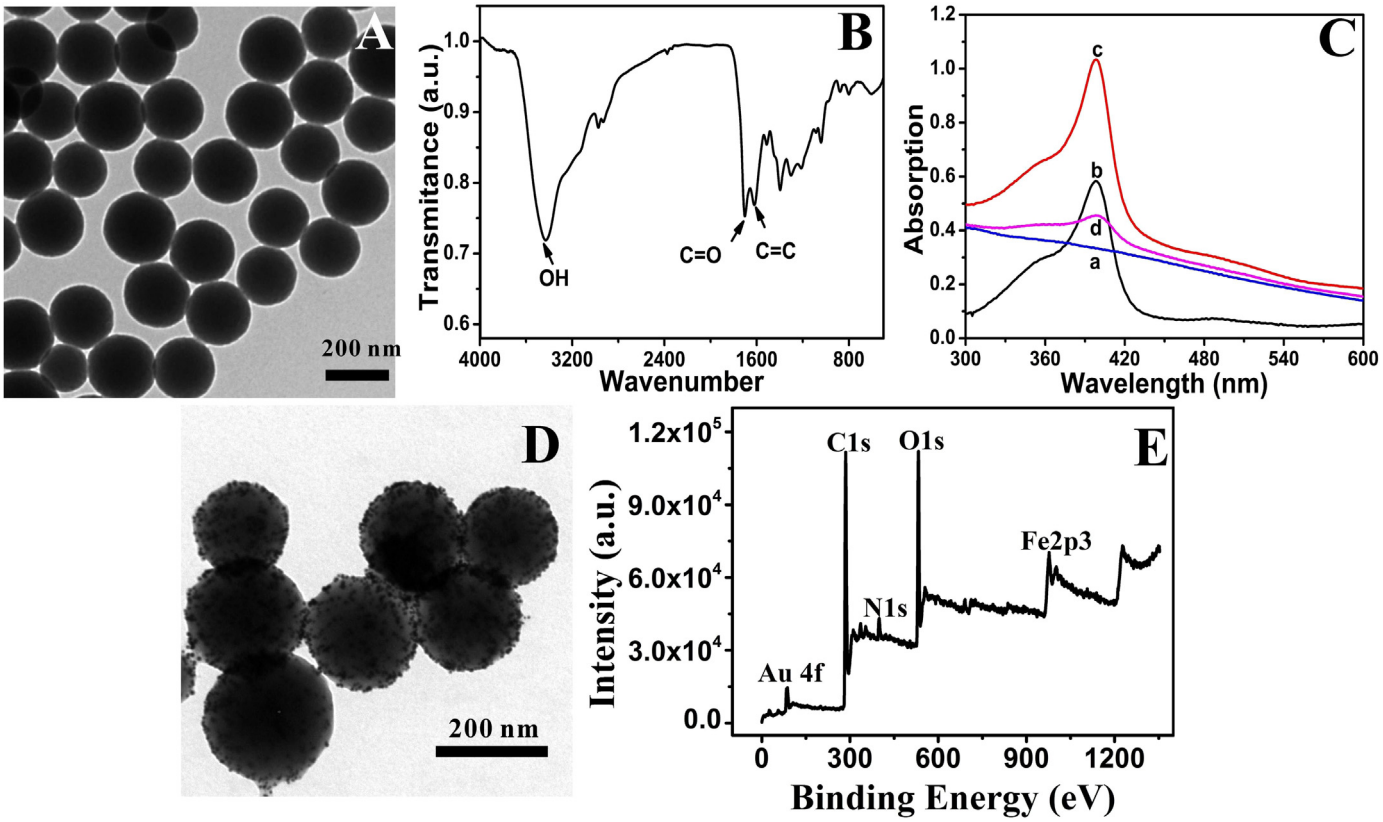

Fig. 1. TEM image of 200 nm carbon spheres prepared at 180 °C for 6 h (A); FTIR spectra of carbon spheres (B); Characterization of hemin-carbon sphere conjugates: a) UV–Vis spectroscopy of carbon spheres in methanol; b) free hemin molecules; c) the mixture of hemin and carbon spheres in methanol; d) CS@hemin conjugate re-dispersed in methanol. All samples show a Soret band at 400 nm (C); TEM image of the composite of CS@hemin/AuNPs (D); XPS spectra of the CS@hemin/AuNPs (E).

3.3. Optimized conditions of the biosensor

To achieve optimal sensing performance, the major parameters were optimized by varying of pH effects on MB degradation and electrochemical measurements, H_2O_2 concentration and immersion time effects on MB degradation. When current responses of the modified electrode at different pH values were investigated (Fig. S4A), the current response increased with increasing pH value, and then reached a peak at pH 7.5. Therefore, pH 7.5 was regarded as the optimal pH.

To our knowledge, pH also had a great influence on the degradation of MB, which was investigated in Fig. S4B. The results revealed that a lower pH was beneficial for MB degradation down to pH 4.5, below which no further change was evident. Meanwhile, the MB/SA/GO hydrogel modified electrode will be unstable when pH is too acidic. Thus, pH 4.5 was chosen as the optimal condition.

Degradation time was also investigated to achieve a maximal change in current response (Fig. S4B). With increasing time, the change in current quickly increased until a time of 15 min, after which degradation time increased more slowly. Therefore, 15 min was selected as the optimal degradation time.

Another important factor for degradation of MB affixed to an electrode was the concentration of H_2O_2 (Fig. S4C). The immunosensor fabricated here was studied in PBS containing H_2O_2 concentrations within the range of 0.01–0.12 M. A maximum current change response was obtained when the H_2O_2 concentration was 0.01 M. Thus, 0.1 M was selected as the optimal H_2O_2 concentration.

3.4. Analytical performance

Under optimal experimental conditions, square wave voltammetric

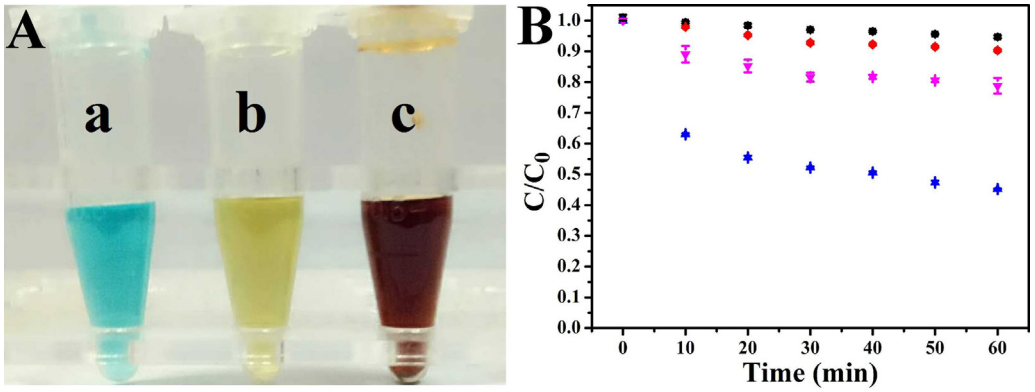

Fig. 2. Visual color changes during the oxidation of a) TMB (10 mM HAC-NaAC buffer, pH = 5.0), b) DAB (10 mM NaAc buffer, pH 6.0), c) OPD (PBS buffer, 10 mM, pH =7.4), containing 100 mM H_2O_2 in the presence of CS@hemin. (A); Concentration changes of MB under different conditions: (a) H_2O_2; (b) hemin and H_2O_2; (c) CS@hemin; (d) CS@hemin and H_2O_2. Reactions a-d were done at pH 7.0 (PBS), T = 25 °C, [MB] = 50 μM, [H_2O_2] = 50 mM, [hemin] = 30 μM, [CS@hemin] = 30 μM hemin equivalent.

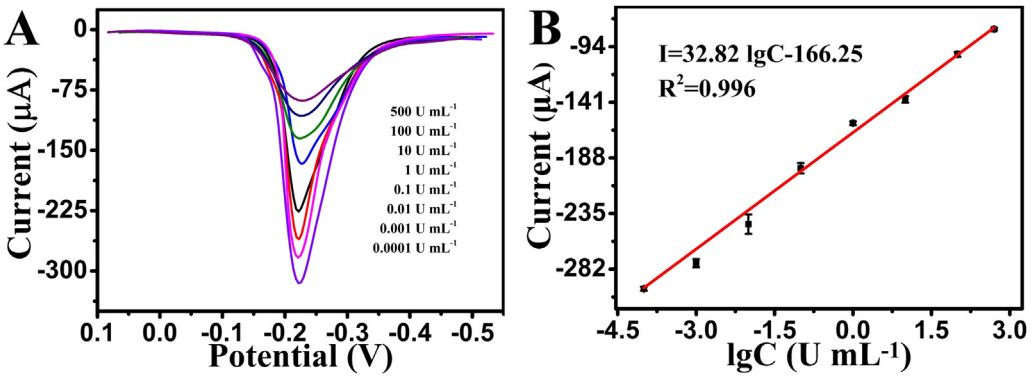

Fig. 3. SWV responses of the biosensors for different concentrations of CA125 (A); linear calibration curve of current responses and the logarithm of different concentrations of CA125 (B).

(SWV) was used to measure preparations with different CA125 concentrations. As shown in Fig. 3, the current response of the biosensor decreased with increasing CA125 concentration because as CA125 concentration increased, more labels were captured to accelerate degradation of the signal species. The calibration plot exhibited a good linear relationship between peak current and the logarithm of CA125 concentration within the range 0.1 mU mL^{-1} to 500 U mL^{-1} with a correlation coefficient of 0.996. Quantitative CA125 determination was obtained using the linear equation of I= 32.82lgC-166.25 with a detection limit of 0.048 mU mL^{-1} (S/N = 3).

3.5. Selectivity, reproducibility, and stability of this immunosensor

Several potential interferences, including CA199, CA242, HSA, IgG and glucose were selected to investigate the selectivity of the biosensor based on the following analyte characteristics: CA199 and CA242 were selected as analyte competitors in this work because they are also forms of carbohydrate antigens and their normal concentrations in the human body are 0–40 U mL^{-1} and 0–20 U mL^{-1}, respectively; IgG is the most common type of antibody found in blood circulation, representing approximately 75% of serum antibodies in humans; As for HSA and glucose, they are present in high amounts in human serum. Fig. S6 showed that CA125 (0.01 U mL^{-1}) triggered a remarkable signal, while no obvious signal was observed for the other samples, indicating that this sensor possessed a good selectivity.

Five modified electrodes prepared independently under the same conditions were used to evaluate sensor reproducibility (CA125, 0.01 U mL^{-1}). Values close to a relative standard deviation (RSD) value of 3.6% (n = 5) were obtained with the five sensors, confirming that sensors exhibited good reproducibility.

In order to investigate the sensor stability, a hydrogel modified electrode was stored in a clean, dry, air-tight container and placed in a dark location at 4 °C. After long term storage for 30 days, the RSD value fell within 91.2% of its initial value. The stability of the biosensor was further investigated by plotting CV curves of (Fig. S7) the biosensor at scan rates of 50 mV s^{-1} over 20 cycles. As shown in Fig. S7, the MB/Ca^{2+}/SA/GO/GCE exhibited a slightly decreasing peak current with the increase in cycle number. These results illustrate that the sensor exhibited good stability.

3.6. Real sample analysis

Finally, in order to evaluate the suitability of the immunosensor in a clinical setting, recovery experiments were performed by spiking serum samples with CA125 at various concentrations. For CA125 at concentrations of 0.008, 0.016, 10, 30 and 60 U mL^{-1}, good agreement was observed between the predicted and measured values of the CA125 concentrations (Table S1). The recoveries were achieved to be in the range of 103.37–109.20%, suggesting good performance for detection of analyte within the serum samples. Indeed, a CA125 detection limit as low as 0.048 mU mL^{-1} (S/N = 3) was achieved, over six orders of magnitude more sensitive than achieved using conventional ELISA. Moreover, this immunosensor exhibited performance superior to that of previously developed CA125 electrochemical immunosensors with good reliability and sensitive and specific detection of CA125 present within clinical samples. (Table S2).

4. Conclusion

In summary, we demonstrated an improved ELISA incorporating an electro-readout mode in place of the conventional colorimetric readout mode using a system based on CS@hemin triggered degradation of MB. Compared with traditional ELISA, the improved ELISA exhibited greater sensitivity and appreciable time savings. Moreover, the improved ELISA achieved a satisfactory detection performance with a LOD of 0.048 mU mL^{-1}, a value over six orders of magnitude lower than that of conventional ELISA for CA125 detection. These results illustrate that this degradation-based readout method represented a winning combination of electro signal readout mode and classical ELISA. This methodology offers a significant model for protein detection and provides a promising choice for convenient, rapid, sensitive and affordable biomolecular quantitation for clinical applications. In addition, whole blood sample should be a better choice than human serum sample for detection of biomarker because it can provide much higher clinical relevance of tumor. However, untreated whole blood sample always cannot be detected directly by traditional ELISA due to its serious interferences from inhibitors and cells. If relevant issues can be overcome, present method could be used to detect the biomarker in blood more quickly and accurately.

Acknowledgement

This research was financed by grants from National Natural Science Foundation of China (21673143, 21273153), Natural Science Foundation of Beijing Municipality (2172016, 2132008), High-level Teachers in Beijing Municipal Universities in the Period of 13th Five-year Plan (IDHT20180517) and Capacity Building for Sci-Tech Innovation - Fundamental Scientific Research Funds (025185305000/195).

Declaration of interest statement

The authors declare no conflict of interest.

Appendix A. Supplementary material

Supplementary data associated with this article can be found in the online version at doi:10.1016/j.bios.2018.11.038.

References

Al-Ogaidi, I., Aguilar, Z.P., Suri, S., Gou, H., Wu, N., 2013. Dual detection of cancer biomarker CA125 using absorbance and electrochemical methods. Analyst 138, 5647–5653.

Arya, S.K., Estrela, P., 2018. Electrochemical ELISA-based platform for bladder cancer protein biomarker detection in urine. Biosens. Bioelectron. 117, 620–627.

Bui, M.-P.N., Ahmed, S., Abbas, A., 2015. Single-digit pathogen and attomolar detection with the naked eye using liposome-amplified plasmonic immunoassay. Nano Lett. 15, 6239–6246.

Chen, F., Hou, S., Li, Q., Fan, H., Fan, R., Xu, Z., Zhala, G., Mai, X., Chen, X., Chen, X., Liu, Y., 2014. Development of atom transfer radical polymer-modified gold nanoparticle-based enzyme-linked immunosorbent assay (ELISA). Anal. Chem. 86, 10021–10024.

Clement, F., Dewar, V., Van Braeckel, E., Desombere, I., Dewerchin, M., Swysen, C., Demoitié, M.-A., Jongert, E., Cohen, J., Leroux-Roels, G., Cambron, P., 2012. Validation of an enzyme-linked immunosorbent assay for the quantification of human IgG directed against the repeat region of the circumsporozoite protein of the parasite Plasmodium falciparum. Malar. J. 11, 384.

Garcia-Viloca, M., Gao, J., Karplus, M., Truhlar, D.G., 2004. How enzymes work: analysis by modern rate theory and computer simulations. Science 303, 186.

Guo, Y., Deng, L., Li, J., Guo, S., Wang, E., Dong, S., 2011. Hemin–graphene hybrid nanosheets with intrinsic peroxidase-like activity for label-free colorimetric detection of single-nucleotide polymorphism. ACS Nano 5, 1282–1290.

Hermsen, B.B.J., Mensdorff-Pouilly, Sv, Berkhof, J., Diest, P.Jv, Gille, J.J.P., Menko, F.H., Blankenstein, M.A., Kenemans, P., Verheijen, R.H.M., 2007. Serum CA-125 in Relation to Adnexal Dysplasia and Cancer in Women at Hereditary High Risk of Ovarian Cancer. J. Clin. Oncol. 25, 1383–1389.

Huang, X., Chen, R., Xu, H., Lai, W., Xiong, Y., 2016. Nanospherical brush as catalase container for enhancing the detection sensitivity of competitive plasmonic ELISA. Anal. Chem. 88, 1951–1958.

Jiang, B., Dai, D., Yao, Y., Xu, T., Li, R., Xie, R., Chen, L., Chen, W., 2016. The coupling of hemin with persistent free radicals induces a nonradical mechanism for oxidation of pollutants. Chem. Commun. 52, 9566–9569.

Juang, D.S., Lin, C.-H., Huo, Y.-R., Tang, C.-Y., Cheng, C.-R., Wu, H.-S., Huang, S.-F., Kalnitsky, A., Lin, C.-C., 2018. Proton-ELISA: electrochemical immunoassay on a dual-gated ISFET array. Biosens. Bioelectron. 117, 175–182.

Kim, J., Cote, L.J., Kim, F., Huang, J., 2010. Visualizing graphene based sheets by fluorescence quenching microscopy. J. Am. Chem. Soc. 132, 260–267.

Li, Y., Du, Q., Liu, T., Sun, J., Wang, Y., Wu, S., Wang, Z., Xia, Y., Xia, L., 2013. Methylene blue adsorption on graphene oxide/calcium alginate composites. Carbohydr. Polym. 95, 501–507.

Li, Y., Wu, J., Zhang, C., Chen, Y., Wang, Y., Xie, M., 2017. Manganese dioxide nanoparticle-based colorimetric immunoassay for the detection of alpha-fetoprotein. Microchim. Acta 184, 2767–2774.

Linardy, E.M., Erskine, S.M., Lima, N.E., Lonergan, T., Mokany, E., Todd, A.V., 2016. EzyAmp signal amplification cascade enables isothermal detection of nucleic acid and protein targets. Biosens. Bioelectron. 75, 59–66.

Luo, L., Song, Y., Zhu, C., Fu, S., Shi, Q., Sun, Y.-M., Jia, B., Du, D., Xu, Z.-L., Lin, Y., 2018. Fluorescent silicon nanoparticles-based ratiometric fluorescence immunoassay for sensitive detection of ethyl carbamate in red wine. Sens. Actuat B-Chem. 255, 2742–2749.

Ma, X., Wang, M.-C., Feng, J., Zhao, X., 2015. Aspect ratio control of Au nanorods via covariation of the total amount of $HAuCl_4$ and ascorbic acid. J. Alloy. Compd. 637, 36–43.

Qu, Z., Xu, H., Xu, P., Chen, K., Mu, R., Fu, J., Gu, H., 2014. Ultrasensitive ELISA using enzyme-loaded nanospherical brushes as labels. Anal. Chem. 86, 9367–9371.

Sakaki, T., Shibata, M., Miki, T., Hirosue, H., Hayashi, N., 1996. Reaction model of cellulose decomposition in near-critical water and fermentation of products. Bioresour. Technol. 58, 197–202.

Shao, F., Jiao, L., Miao, L., Wei, Q., Li, H., 2017. A pH Indicator-linked Immunosorbent assay following direct amplification strategy for colorimetric detection of protein biomarkers. Biosens. Bioelectron. 90, 1–5.

Sok, D., Clarizia, L.-J.A., Farris, L.R., McDonald, M.J., 2009. Novel fluoroimmunoassay for ovarian cancer biomarker CA-125. Anal. Bioanal. Chem. 393, 1521–1523.

Sun, X., Li, Y., 2004. Colloidal carbon spheres and their core/shell structures with noble-metal nanoparticles. Angew. Chem. Int. Ed. 43, 597–601.

Tang, Z., Ma, Z., 2017. Multiple functional strategies for amplifying sensitivity of amperometric immunoassay for tumor markers: a review. Biosens. Bioelectron. 98, 100–112.

Thakur, S., Pandey, S., Arotiba, O.A., 2016. Development of a sodium alginate-based organic/inorganic superabsorbent composite hydrogel for adsorption of methylene blue. Carbohydr. Polym. 153, 34–46.

Vallée-Bélisle, A., Ricci, F., Uzawa, T., Xia, F., Plaxco, K.W., 2012. Bioelectrochemical Switches for the Quantitative Detection of Antibodies Directly in Whole Blood. J. Am. Chem. Soc. 134, 15197–15200.

Wang, X., Hou, C., Qiu, W., Ke, Y., Xu, Q., Liu, X.Y., Lin, Y., 2017. Protein-directed synthesis of bifunctional adsorbent-catalytic hemin-graphene nanosheets for highly efficient removal of dye pollutants via synergistic adsorption and degradation. ACS Appl. Mater. Interfaces 9, 684–692.

Wang, Y., Liu, Y., Deng, X., Cong, Y., Jiang, X., 2016. Peptidic β-sheet binding with Congo Red allows both reduction of error variance and signal amplification for immunoassays. Biosens. Bioelectron. 86, 211–218.

Wang, Y., Zhao, G., Wang, H., Cao, W., Du, B., Wei, Q., 2018. Sandwich-type electrochemical immunoassay based on Co_3O_4@MnO_2-thionine and pseudo-ELISA method toward sensitive detection of alpha fetoprotein. Biosens. Bioelectron. 106, 179–185.

Wei, H., Wang, E., 2013. Nanomaterials with enzyme-like characteristics (nanozymes): next-generation artificial enzymes. Chem. Soc. Rev. 42, 6060–6093.

Xu, Q., Yan, F., Lei, J., Leng, C., Ju, H., 2012. Disposable electrochemical immunosensor by using carbon sphere/gold nanoparticle composites as labels for signal amplification. Chem. Eur. J. 18, 4994–4998.

Xue, T., Jiang, S., Qu, Y., Su, Q., Cheng, R., Dubin, S., Chiu, C.-Y., Kaner, R., Huang, Y., Duan, X., 2012. Graphene-supported hemin as a highly active biomimetic oxidation catalyst. Angew. Chem. Int. Ed. 51, 3822–3825.

Yao, Y., Jiang, B., Mao, Y., Chen, J., Huang, Z., Huang, S., Zhang, L., 2015. Extremely enhanced contaminant decomposition catalyzed by hemin via the coupling of persistent free radicals and ascorbic acid. Chem. Commun. 51, 16139–16142.

Yao, Y., Mao, Y., Huang, Q., Wang, L., Huang, Z., Lu, W., Chen, W., 2014. Enhanced decomposition of dyes by Hemin-ACF with significant improvement in pH tolerance and stability. J. Hazard. Mater. 264, 323–331.

Ye, H., Yang, K., Tao, J., Liu, Y., Zhang, Q., Habibi, S., Nie, Z., Xia, X., 2017. An enzyme-free signal amplification technique for ultrasensitive colorimetric assay of disease biomarkers. ACS Nano 11, 2052–2059.

Yu, X., Zhang, X., Wang, Z., Jiang, H., Lv, Z., Shen, J., Xia, G., Wen, K., 2018. Universal simultaneous multiplex ELISA of small molecules in milk based on dual luciferases. Anal. Chim. Acta 1001, 125–133.

Zhang, D., Li, W., Ma, Z., 2018a. Improved sandwich-format electrochemical immunosensor based on “smart” SiO_2@polydopamine nanocarrier. Biosens. Bioelectron. 109, 171–176.

Zhang, J., Zhuang, J., Gao, L., Zhang, Y., Gu, N., Feng, J., Yang, D., Zhu, J., Yan, X., 2008. Decomposing phenol by the hidden talent of ferromagnetic nanoparticles. Chemosphere 73, 1524–1528.

Zhang, L., Fan, C., Liu, M., Liu, F., Bian, S., Du, S., Zhu, S., Wang, H., 2018b. Biominerized gold-Hemin@MOF composites with peroxidase-like and gold catalysis activities: a high-throughput colorimetric immunoassay for alpha-fetoprotein in blood by ELISA and gold-catalytic silver staining. Sens. Actuat B-Chem. 266, 543–552.

Zhu, Z., Guan, Z., Jia, S., Lei, Z., Lin, S., Zhang, H., Ma, Y., Tian, Z.Q., Yang Chaoyong, J., 2014. Au@Pt nanoparticle encapsulated target-responsive hydrogel with volumetric bar-chart chip readout for quantitative point-of-care testing. Angew. Chem. Int. Ed. 53, 12503–12507.